AIAA JOURNAL
Vol. 42, No. 7, July 2004

Numerical Simulation of Stack–Heat Exchangers Coupling in a Thermoacoustic Refrigerator

David Marx* and Philippe Blanc-Benon†
Ecole Centrale de Lyon, 69134 Ecully, France

The Navier–Stokes equations for an unsteady and compressible flow are solved numerically to investigate the flow near the stack of a thermoacoustic refrigerator. The computational domain is a resonator "slice" including the resonator end but not the source. An incoming wave is introduced into the domain using the method of characteristics. Also included in the domain is a stack plate and two heat exchangers. The effects of the acoustic Mach number and geometrical parameters on refrigerator performance is investigated. Of special interest are some nonlinear temperature oscillations, which are not predicted by linear models and are due to acoustic propagation, and coupling between the stack plate and the heat exchangers. It is shown that the maximum heat pumping occurs for a stack/heat exchanger separation that is of the order of one particle displacement amplitude.

Introduction

EXAMPLES of thermoacoustic heat engines include, among others, Sondhauss oscillations.[1] These were observed over 100 years ago by glassblowers who noticed that when a hot glass bulb is attached to a cool stem, the stem tip sometimes emits a sound. In such a system, thermal energy is converted into sound, which corresponds to a prime mover. The generated sound can be either a traveling wave or a standing wave. Heat-pumping devices utilizing acoustic energy can also be fabricated. These are termed thermoacoustic refrigerators. Both types of thermoacoustic engines, prime movers and heat pumps, have been described in a unified fashion by Swift.[1]

Thermoacoustic heat pumping is a second-order phenomenon resulting from the interaction between two first-order acoustic perturbations. As an example, consider a plane-traveling acoustic wave propagating in a fluid at rest. The first-order temperature and velocity associated with the plane wave are T_1 and u_1, respectively. These two quantities oscillate in phase, so that the time average $\langle T_1 u_1 \rangle_t$ (where $\langle\ \rangle_t$ is the time average operator) is a nonzero quantity. Hence, the sound wave carries a second-order (as a product of two first-order quantities) mean enthalpy flux $\langle \rho_0 c_p T_1 u_1 \rangle_t$, where ρ_0 is the density of the fluid at rest and c_p is the isobaric specific heat of the fluid. In normal conditions, T_1 and u_1 are small and the mean enthalpy flux is negligible. It is possible to obtain much stronger values for T_1 and u_1 within an acoustic resonator driven at high amplitudes. Of course, in an ideal resonator a standing wave is formed for which $\langle T_1 u_1 \rangle_t$ is nearly zero. But the addition of a stack of tightly spaced plates aligned with the resonator axis allows a phasing in the stack such that $\langle T_1 u_1 \rangle_t \neq 0$, while both u_1 and T_1 are large. Hence, there is a significant mean enthalpy flux along the stack that can be used to pump heat from a cold heat exchanger into a hot heat exchanger, which is the basic principle of thermoacoustic refrigerators.

Thermoacoustic refrigerators are relatively recent; they have been developed since the early 1980s. They are environmentally benign and offer an alternative to traditional systems based on refrigerants such as chlorofluorocarbons, which have already been phased out due to environmental concerns, or hydrochlorofluorocarbons, which soon will be. Also their miniaturization is possible and would provide small-size refrigerators. A disadvantage is that the coefficient of performance of such devices is still low, typically 20% of the Carnot coefficient of performance.[2] Better performance, 40% of the Carnot efficiency, has been reached recently for a thermoacoustic Stirling heat engine.[3] To improve efficiency, it is necessary to better understand nonlinear effects,[4] including second-order effects such as streaming[5] (mean flow motions that accompany acoustic waves in a resonator) and heat transfer from the stack to the heat exchangers. The investigation of nonlinear effects is important because these are not taken into account within the framework of available linear theory, which is based on a linearization of the fundamental equations.[1] Nonlinear effects (harmonic generation) in prime movers have been frequently reported and are due, among other things, to nonlinear wave propagation at high amplitudes in the resonator.[6] In the refrigerator case, departures from linear theory have been reported even at moderate amplitudes.[7,8] In the simulation by Worlikar and Knio,[8] such departure is observed despite the fact that the resonator is not included in the simulation. Hence, nonlinear phenomena are probably not only due to propagation in the resonator and further investigations are required. Also lacking is a design methodology for heat exchangers.

Numerical simulations of thermoacoustic devices have already been performed. Cao et al.[9] simulated an isothermal zero-thickness plate in a standing wave by solving the compressible unsteady two-dimensional Navier–Stokes equations. A very similar simulation has been done recently by Ishikawa and Mee.[10] Worlikar and Knio[11] have simplified the governing equations using a low-Mach-number approach to simulate a plate of finite thickness, including heat exchangers in contact with the stack plates.[8] This work, and a study of heat exchangers detached from the stack plates, has been completed by Besnoin.[12] The flow at the edges of the plate obtained using their simulations was found to be in good agreement with experimental observations.[13] Karpov and Prosperetti[14] have combined a nonlinear one-dimensional formulation and a numerical simulation to study thermoacoustic devices of variable cross section. The effects of cross-sectional variation on wave nonlinearity have also been investigated by Hamilton et al.,[15] but using a two-dimensional formulation and zero-thickness stack plates. Both studies confirmed the importance of nonlinear wave propagation in the resonator. Finally, Boluriaan and Morris[16] performed a numerical study of minor losses through a sudden contraction in an acoustic resonator.

In the present study, numerical simulations of the flow in a portion of a half-wavelength cooler were performed. The role of zero-thickness stack plates and heat exchangers was investigated. The choice of a high operating frequency was made to reduce

Presented as Paper 2003-3150 at the 9th AIAA–CEAS Aeroacoustic Conference, Hilton Head, SC, 12–14 May 2003; received 4 August 2003; revision received 31 January 2004; accepted for publication 8 February 2004.

*Ph.D. Student, Laboratoire de Mécanique des Fluides et d'Acoustique, UMR 5509, Centre Acoustique; currently Research Associate, School of Engineering, University of Manchester, Oxford Road, Manchester, England M13 9PL, United Kingdom; david.marx@ec-lyon.fr. Member AIAA.

†Researcher, Laboratoire de Mécanique des Fluides et d'Acoustique, UMR 5509, Centre National de la Recherche Scientifique.

computational effort. Results were obtained first in the case of an isothermal plate, and second in the case of a nonisothermal plate without heat exchangers. Nonlinear behavior not predicted by linear theory was observed in the stack at high Mach numbers. In particular, temperature oscillation harmonics not due to acoustic nonlinear propagation were observed. Finally, heat exchangers were included and the effect of geometrical parameters on refrigerator coefficient of performance was investigated. Particularly, it was found that one specific value of the heat exchanger length, and for the gap between heat exchangers and stack plates, yields a maximum efficiency.

Numerical Model

Geometry and Computational Domain

The geometry of the thermoacoustic refrigerator under consideration is shown in Fig. 1. The system includes a resonator, an acoustic driver, a hot heat exchanger, a stack, and a cold heat exchanger. The operating frequency f is related to the wavelength λ through $\lambda = c/f$, where c is the sound speed. The wave number is $k = 2\pi/\lambda$. The length of the resonator, l, is one-half the wavelength λ. The driver is located at $x = 0$, and the stack plates center is at $x = x_s$. The complete simulation of an entire thermoacoustic refrigerator is prohibitively expensive, and so the simulation was performed on the reduced computational domain, referred to as CD in Fig. 1, and shown in more detail in Fig. 2. It is a two-dimensional domain, which includes the resonator end, a zero-thickness stack plate boundary (surface S_{plate}), a zero-thickness cold heat exchanger boundary (surface S_c), and a zero-thickness hot heat exchanger boundary (surface S_h). Only one plate was included because the structure is assumed to be periodic in the y direction. The lengths of the stack plate, the cold heat exchanger, and the hot heat exchanger are L, L_c, and L_h, respectively. The gap between the cold heat exchanger and the plate is G_c. The gap between the hot heat exchanger and the plate is G_h. The height of the domain, y_0, is one-half the distance between two stack plates. In the following, $L = \lambda/40$ unless specified otherwise.

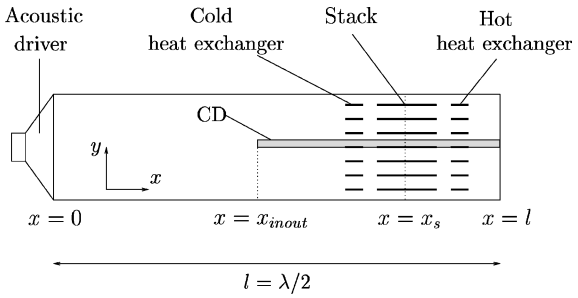

Fig. 1 Schematic of a thermoacoustic refrigerator.

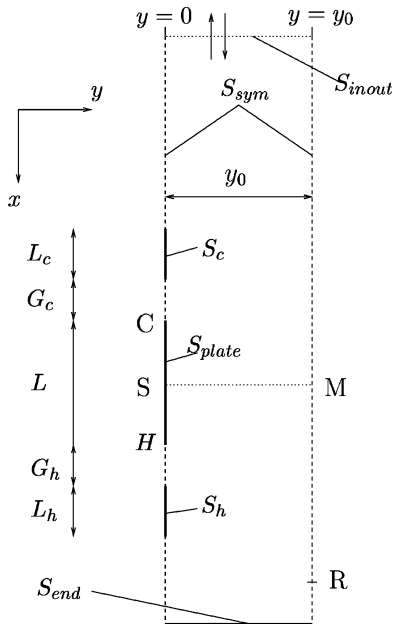

Fig. 2 Computational domain referred to as region CD in Fig. 1.

Boundary Conditions

On the boundaries S_{sym} (dashed lines in Fig. 2), symmetry boundary conditions were imposed. This is expressed by

$$\left.\begin{aligned}\frac{\partial \phi}{\partial y} &= 0\\ v &= 0\end{aligned}\right\} \quad \text{on } S_{\text{sym}} \tag{1}$$

where ϕ is one of the following variables: the pressure p; the temperature T; the density ρ, or the velocity in the x direction, u. The velocity in the y direction is v. The velocity vector is $\boldsymbol{u} = (u, v)$. A nonslip boundary condition was imposed on the solid surfaces S_{end}, S_{plate}, and S_c. The end of the resonator was an adiabatic wall, and each heat exchanger was treated as an isothermal wall. On the plate surface, the fluid temperature was the same as that of the plate. Hence, the following boundary conditions were enforced:

$$\left.\begin{aligned}u = v &= 0\\ \frac{\partial T}{\partial x} &= 0\end{aligned}\right\} \quad \text{on } S_{\text{end}} \tag{2}$$

$$\left.\begin{aligned}u = v &= 0\\ T &= T_c\end{aligned}\right\} \quad \text{on } S_c \tag{3}$$

$$\left.\begin{aligned}u = v &= 0\\ T &= T_h\end{aligned}\right\} \quad \text{on } S_h \tag{4}$$

$$\left.\begin{aligned}u = v &= 0\\ T &= T_s\end{aligned}\right\} \quad \text{on } S_p \tag{5}$$

where T_c and T_h are the prescribed temperatures of the cold and hot heat exchangers, respectively, and T_s is the temperature of the solid plate.

Modeling of the acoustic source is a difficult problem. The choice was made not to consider the acoustic driver. Instead, an incoming acoustic wave was introduced into the computational domain through the boundary S_{inout} located at $x = x_{\text{inout}}$ using the method of characteristics. This incident wave travels through the domain, is reflected by the resonator end wall, travels back, and exits through S_{inout}. The superposition of the incident and reflected waves creates a standing wave in the domain. However, this standing wave is not a resonant wave resulting from a wave traveling back and forth between the source and the end of the resonator. The advantage of this method is that the acoustic wave travels in the domain during less than one acoustic cycle. Hence, there is no sufficient time for shock formation or wave steepening, even for large pressure ratios. An alternative method consists of replacing the surface S_{end} by another S_{inout} surface to create a standing wave by superimposing two traveling waves, each one coming from one end of the domain and exiting at the other end. A difficulty would then be to choose the correct phasing between the two traveling waves, a problem that has been encountered by Cao et al.,[9] who needed to adjust the phase to get correct energy flow results.

Computational Cost

Computer simulations of thermoacoustic devices require large amounts of CPU time. This is due to a length-scale disparity. The length scale in the y direction is of the order of the viscous penetration depth δ_v. The length scale in the x direction is the length l of the resonator. This is expressed by

$$y_0 \sim \delta_v, \qquad l \sim \lambda \tag{6}$$

The viscous penetration depth δ_v is defined by

$$\delta_v = \sqrt{\nu\lambda/\pi c} \tag{7}$$

where ν is the kinematic viscosity. In the usual frequency range for thermoacoustic refrigerators (less than 1 kHz), the relation $\lambda/\delta_\nu \sim 10^3$ holds. Let Δx and Δy be the smallest mesh size in the x and y directions and let them be equal. For a precise resolution of the flow between the plates, $\delta_\nu/\Delta x \sim 10$. The number of grid points in the x direction, n_x, satisfies

$$n_x \sim l/\Delta x \sim (\delta_\nu/\Delta x)(\lambda/\delta_\nu) \sim 10^4 \tag{8}$$

Hence, n_x will necessarily be large. Moreover, the Courant–Friedrich–Levy (CFL) stability condition implies that

$$\Delta t < \Delta x/c \sim (\Delta x/\delta_\nu)(\delta_\nu/c) \tag{9}$$

The number of time steps, n_τ, per period τ of the wave is then

$$n_\tau \sim \tau/\Delta t \sim (\delta_\nu/\Delta x)(\lambda/\delta_\nu) \sim 10^4 \tag{10}$$

where the relation $\lambda = c\tau$ was used. Note that n_τ and n_x have a common value. The number of time steps per acoustic cycle is large and unfortunately many acoustic cycles must be calculated before a steady state is reached. Hence, unless a strategy is used to circumvent the CFL stability condition,[15] using for example a low-Mach-number method,[11,17] the computational cost is high. This was the case in the present simulation. This cost can nevertheless be reduced in two different ways. The first is to reduce as much as possible the size of the computational domain, as discussed earlier. The second is to simulate a high-frequency device: because both n_x and n_τ depend on λ/δ_ν, which is proportional to $\sqrt{\lambda}$, the computational cost ($\sim n_x n_\tau$) is proportional to λ, which is inversely proportional to the frequency f. In the present simulation, the system was operated at $f = 20$ kHz. This frequency is high but corresponds to miniaturization goals, because the resonator length varies with the wavelength, that is, as the inverse of the frequency. The miniaturization of thermoacoustic refrigerators is attractive for microelectronic device refrigeration and a high-frequency device (about 5 kHz) has been tested recently by Chen et al.[18] This frequency was much greater than those used until now in most experiments (i.e., a few hundred hertz).[1]

Governing Equations

The equation of state for the flow, which is assumed to be an ideal gas, and the conservation equations for the fluid are

$$p = \rho r T \tag{11}$$

$$\frac{\partial \rho}{\partial t} + \nabla \cdot (\rho \boldsymbol{u}) = 0 \tag{12}$$

$$\frac{\partial (\rho \boldsymbol{u})}{\partial t} + \nabla \cdot (\rho \boldsymbol{u}\boldsymbol{u}) + \nabla p = \nabla \cdot \boldsymbol{\tau} \tag{13}$$

$$\frac{\partial T}{\partial t} + \boldsymbol{u} \cdot \nabla T + (\gamma - 1) T \nabla \cdot \boldsymbol{u} = \frac{(\gamma - 1)}{\rho r}[\Phi + \nabla \cdot (K \nabla T)] \tag{14}$$

where r is the gas constant ($r = 287\ \mathrm{JK^{-1}kg^{-1}}$). Components of the viscous stress tensor $\boldsymbol{\tau}$ can be written as

$$\tau_{xx} = \frac{4}{3}\mu\frac{\partial u}{\partial x} - \frac{2}{3}\mu\frac{\partial v}{\partial y}$$

$$\tau_{xy} = \tau_{yx} = \mu\left(\frac{\partial u}{\partial y} + \frac{\partial v}{\partial x}\right)$$

$$\tau_{yy} = \frac{4}{3}\mu\frac{\partial v}{\partial y} - \frac{2}{3}\mu\frac{\partial u}{\partial x} \tag{15}$$

The viscous dissipation Φ is defined by

$$\Phi = 2\mu\left[\left(\frac{\partial u}{\partial x}\right)^2 + \left(\frac{\partial v}{\partial y}\right)^2 + \frac{1}{2}\left(\frac{\partial u}{\partial y} + \frac{\partial v}{\partial x}\right)^2 - \frac{1}{3}\left(\frac{\partial u}{\partial x} + \frac{\partial v}{\partial y}\right)^2\right] \tag{16}$$

where μ is the shear viscosity and K is the thermal conductivity of the fluid. The temperature dependence of μ and K was not taken into account, which is a reasonable approximation because the temperature gradients were small in the present case. In Eqs. (12–14), thermoviscous terms are grouped on the right-hand side to indicate that they are source terms for the thermoacoustic effect.

The temperature of the plate is governed by the energy equation

$$\rho_s c_s \frac{\partial T_s}{\partial t} = \frac{\partial}{\partial x}\left(K_s \frac{\partial}{\partial x} T_s\right) + \frac{K}{E}\left(\frac{\partial T}{\partial y}\right)_{S_{\text{plate}}} \tag{17}$$

where ρ_s, c_s, and K_s are the density, the specific heat, and the thermal conductivity of the plate, respectively. The temperature dependence of all solid properties was ignored. The second term on the right-hand side of Eq. (17) is a source term for the plate, which results from energy exchange with the fluid and also takes into account the heat flux continuity at the fluid/solid interface. The length E is the actual thickness of the plate. This means that one-dimensional equation (17) is the average over y of a two-dimensional energy equation for a plate of finite thickness E. Here, E characterizes the heat capacity of the plate. Such a model equation was first used by Schneider et al.[17] and Besnoin and Knio.[19]

In the following, every variable ψ will be written as

$$\psi = \psi_0 + \psi' \tag{18}$$

where ψ_0 is the uniform value when the system is at rest and ψ' is the perturbation. Decomposition (18) was also used in the code to allow simulations including only the linear terms of the governing equations. In the simulations the following values at rest were used: $T_0 = 298$ K, $p_0 = 10^5$ Pa. The working fluid was air; γ denotes its ratio of specific heats. The isobaric specific heat of the gas is then $c_p = \gamma r/(\gamma - 1)$. The constants' values were prescribed: $\gamma = 1.4$, $\nu = 1.5\,10^{-5}\ \mathrm{m^2 s^{-1}}$, $K = 2.5\,10^{-2}\ \mathrm{WK^{-1}m^{-1}}$. For the plate, the properties of Mylar were used: $K_s = 0.14\ \mathrm{WK^{-1}m^{-1}}$, $\rho_s = 1.35\,10^3\ \mathrm{kgm^{-3}}$, $c_s = 1.3\,10^3\ \mathrm{JK^{-1}kg^{-1}}$. The speed of sound, c_0, is defined by $c_0 = \sqrt{(\gamma r T_0)}$, and its value is $c_0 = 346\ \mathrm{ms^{-1}}$.

Numerical Methods

Equations (12–14) and (17) were advanced in time using an explicit, fourth-order Runge–Kutta method. Spatial derivatives were calculated using fourth-order finite differences. Selective filtering[20] was used to suppress grid-to-grid oscillations. For most calculations, a uniform mesh size $\Delta y = \delta_\nu/6$ was used in the y direction. For calculations corresponding to Fig. 6, this value was decreased down to $\Delta y = \delta_\nu/23$ because the height of the channel is small. Above the plate and heat exchangers, a regular mesh size $\Delta x = \Delta y$ was used in the x direction. Outside the heat exchangers, the mesh size in the x direction was stretched with a 5% rate until $\Delta x = 20\Delta y$ was reached: then the mesh size was regular again. Typically, 30 grid points were used in the y direction, and 400 grid points were used in the x direction. Further details about the numerical simulations, as well as a grid refinement study, may be found elsewhere.[21]

Results for an Isothermal Plate

In this section the case of an isothermal plate without heat exchangers is discussed. A uniform $T_s = T_0$ was imposed, where T_0 is the ambient temperature. Such a condition was used in earlier studies.[9,10] Such a boundary condition is not very realistic because there is usually a temperature gradient in the stack plate due to thermoacoustic heat pumping. Nevertheless, this condition allows us to obtain a thermoacoustic heat pumping. It also allows a mean temperature gradient to develop in the fluid above the plate (in the x direction), although it remains small. From a computational point of view, an isothermal plate is attractive because a shorter time is necessary to reach a steady state in the plate, so that computations are not too costly; 50 acoustic cycles were sufficient to reach a steady state. Moreover, this simple problem allowed the study of important phenomena, such as the effects of channel height and of the Mach number, defined by

$$M_a = u_A/c_0 \tag{19}$$

where u_A is the maximum amplitude of the acoustic velocity in the resonator. The Mach number is an important parameter representative of the power of the device. Standard linear theory is expected to be valid for low Mach numbers (typically less than a few percent), whereas nonlinear effects not taken into account by linear theory are expected at higher Mach numbers (see the Introduction).

First the velocity and temperature profiles above the plate in the presence of the acoustic standing wave were investigated. These profiles are important because their temporal average supplies the mean enthalpy flux along the plate. The parameters of the simulation were $kx_s = 2.13$, $\delta_\kappa / y_0 = 0.37$. A low value of the Mach number $M_a = 0.005$ was used. Figures 3 and 4 show the instantaneous velocity and temperature profiles in section SM (see Fig. 2) at different times within one acoustic period. They are compared with the following analytical expressions:

$$u' = \mathrm{Re}\left(\tilde{u}_M \left\{1 - \frac{\cosh[(1+i)(y-y_0)/\delta_v]}{\cosh[(1+i)y_0/\delta_v]}\right\} e^{i\omega t}\right) \quad (20)$$

$$T' = \mathrm{Re}\left(\tilde{T}_M \left\{1 - \frac{\cosh[(1+i)(y-y_0)/\delta_\kappa]}{\cosh[(1+i)y_0/\delta_\kappa]}\right\} e^{i\omega t}\right) \quad (21)$$

where Re denotes the real part. In Eq. (21), δ_κ is the thermal boundary layer, given by

$$\delta_\kappa = \sqrt{\kappa \lambda / \pi c} \quad (22)$$

where $\kappa = K/(\rho c_p)$. Expressions (20) and (21) can be obtained from Swift[1] by setting the mean temperature gradient in the fluid equal to zero, which is a good approximation in the present calculation for the isothermal plate at a low Mach number. Analytical expressions are given for a domain of height y_0, for which nonslip and isothermal boundary conditions are imposed at $y = 0$ and a symmetry condition is imposed at $y = y_0$. The quantities $\tilde{u}_M$ and $\tilde{T}_M$ are complex amplitudes. They were provided by the simulation. Numerical results and theoretical predictions in Figs. 3 and 4 are in very good agreement. This shows that viscous and thermal boundary layer are well resolved using six points per viscous penetration depth, consistent with an earlier study by Besnoin and Knio.[19]

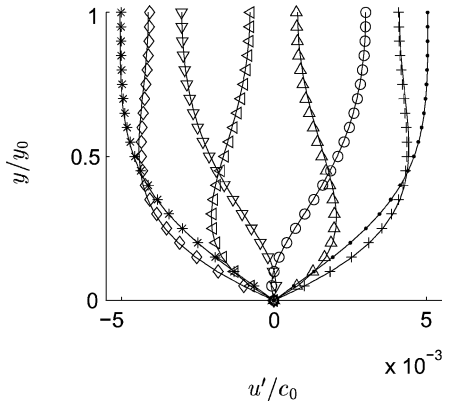

Fig. 3 Instantaneous velocity profiles in section SM (see Fig. 2) at different times within one period τ: ○, $t = 0$; ◁, $t = \tau/8$; ◇, $t = 2\tau/8$; ∗, $t = 3\tau/8$; ∇, $t = 4\tau/8$; △, $t = 5\tau/8$; +, $t = 6\tau/8$; and ●, $t = 7\tau/8$; ——, theoretical curves [Eq. (20)].

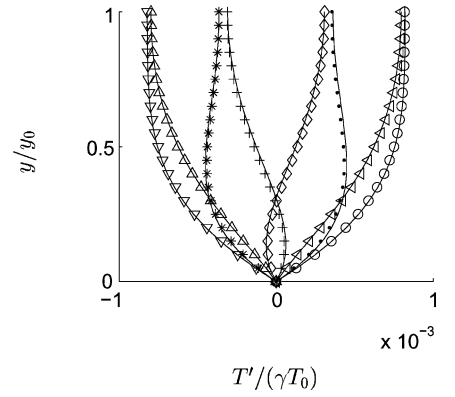

Fig. 4 Instantaneous temperature profiles in section SM (see Fig. 2) at different times within one period τ: ○, $t = 0$; ◁, $t = \tau/8$; ◇, $t = 2\tau/8$; ∗, $t = 3\tau/8$; ∇, $t = 4\tau/8$; △, $t = 5\tau/8$; +, $t = 6\tau/8$; and ●, $t = 7\tau/8$; ——, theoretical curves [Eq. (21)].

As previously mentioned, a mean thermoacoustic enthalpy flux in the x direction, $h_{xm}(y)$, can be written as

$$h_{xm}(y) = \langle \rho_0 c_p u'(y) T'(y) \rangle_t \quad (23)$$

where, for any time-dependent quantity A, the notation $\langle A \rangle_t = A_m$ is used. The flux h_{xm} is directed toward the end of the resonator (S_{end}) and carries heat from edge C of the plate to edge H. It is normalized using $h_0 = \rho_0 c_0^3$. The mean enthalpy flux, h_{xm}, is plotted in Fig. 5 as a function of y/y_0 for different values of the parameter δ_κ / y_0, and for $M_a = 0.02$, $kx_s = 2.13$. The smallest value of δ_κ / y_0, 0.19, corresponds to the case of a large channel compared with boundary-layer thicknesses. The heat flux peaks at a value of $y/y_0 = 0.3$, which corresponds to $y/\delta_\kappa \sim 1.6$. Thus, for a very large channel, the heat flux is carried within a distance of a few thermal boundary-layer thicknesses from the plate, which is well known.[1] For larger values of δ_κ / y_0, the heat flux peaks at $y/y_0 = 1$ in the center of the channel between two stack plates. If δ_κ / y_0 is increased from 0.19 to 0.75 the total flow along the plate increases as well. If δ_κ / y_0 is increased further, the total heat flux decreases. The maximum value of the heat flux is obtained for $\delta_\kappa / y_0 = 0.75$. Similar results were obtained by Cao et al.[9] for values of the parameter δ_κ / y_0 limited to 1.2 due to numerical instabilities.

The mean heat flux in the y direction was investigated, in particular on the plate surface where energy can be carried in the y direction only by heat conduction. The mean heat flux h_{ym} conducted in the y direction is defined by

$$h_{ym} = -K \left\langle \frac{\partial T'}{\partial y} \right\rangle_t \quad (24)$$

The mean heat flux at the plate surface, h_{ym}^{plate}, is the value of h_{ym} obtained from the temperature gradient calculated at the plate. The effect of channel height on h_{ym}^{plate} is shown in Fig. 6, where plots of h_{ym}^{plate} for different values of δ_κ / y_0 are shown. For $h_{ym}^{\mathrm{plate}} > 0$, heat is pumped from the plate to the gas, and for $h_{ym}^{\mathrm{plate}} < 0$, heat is pumped from the gas to the plate. For $\delta_\kappa / y_0 = 1.1$ (and for lower values as well) heat is pumped from the plate at $x = 0$ (edge C) into the plate at $x/L = 1$ (edge H), which is expected. If the value of δ_κ / y_0 is increased, the value of $h_{ym}^{\mathrm{plate}}(x = 0)$ diminishes until it becomes negative for $\delta_\kappa / y_0 > 1.2$. Hence, when the channel height is very small, heat is transferred on both sides of the plate. This surprising result

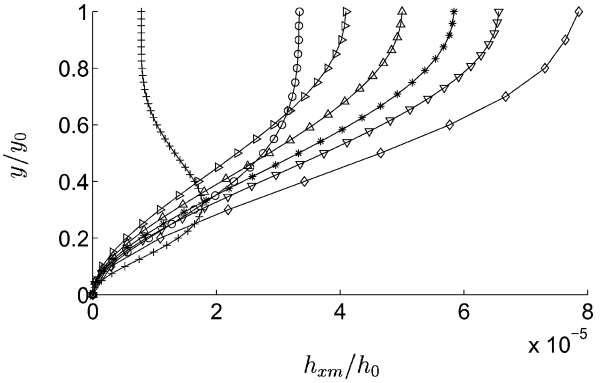

Fig. 5 Mean enthalpy flux h_{xm} in the section SM of Fig. 2 for different values of δ_κ / y_0: +, $\delta_\kappa / y_0 = 0.19$; ○, $\delta_\kappa / y_0 = 0.37$; ◇, $\delta_\kappa / y_0 = 0.75$; ∇, $\delta_\kappa / y_0 = 1.1$; ∗, $\delta_\kappa / y_0 = 1.2$; △, $\delta_\kappa / y_0 = 1.3$; and ▷, $\delta_\kappa / y_0 = 1.45$.

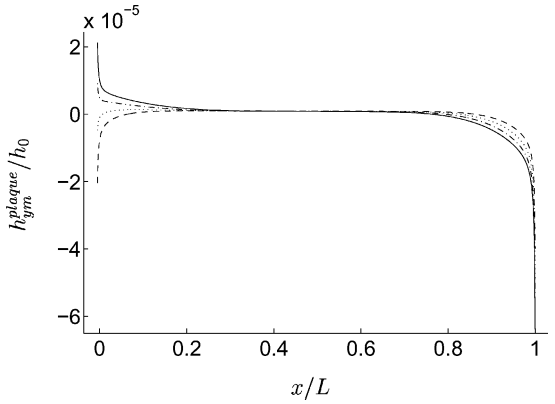

Fig. 6 Mean heat flux at the plate, $h_{ym}^{\text{plate}}(x)$, for different values of δ_κ/y_0; origin $x=0$ at the edge C of the plate; ——, $\delta_\kappa/y_0=1.1$; - - - -, $\delta_\kappa/y_0=1.2$; · · · ·, $\delta_\kappa/y_0=1.3$; and – – –, $\delta_\kappa/y_0=1.45$.

was also reported by Ishikawa and Mee,[10] who attributed the heating to enhanced viscous dissipation for small channel heights. This hypothesis does not explain why h_{ym}^{plate} is positive even in the center of the plate where the dissipation is very high. Calculations made without including the viscous dissipation term [Φ in Eq. (14)] yield the same sign reversal of $h_{ym}^{\text{plate}}(x=0)$ when y_0 becomes very small; therefore, such sign reversal could simply be due to end effects.

As mentioned in the Introduction, nonlinear effects are important in thermoacoustic refrigerators, and so the effect of Mach number variation on the performance of the system was investigated. The total (that is, summed over a section) mean enthalpy carried along the plate, H_{xm}, is

$$H_{xm}=\int_{y=0}^{y=y_0} h_{xm}(y)\,\mathrm{d}y \tag{25}$$

where the integration is performed over section SM (see Fig. 2). The quantity H_{xm} is a measure of the heat transported by thermoacoustic pumping along the plate. It is normalized using $H_0=h_0\delta_v$. A simulation was performed with $\delta_\kappa/y_0=0.37$, $kx_s=2.13$, and $L=\lambda/40$. The enthalpy flux H_{xm} is plotted vs the Mach number in Fig. 7. The dotted line corresponds to an M_a^2 function that fits the calculated curve at low Mach numbers. For $M_a<0.04$, H_{xm} varies as M_a^2. Such a dependence is expected from linear theory. At high Mach numbers, however, H_{xm} varies as M_a. To understand the reason for this change of behavior, the velocity and temperature were monitored at two locations in the computational domain: at point M above the stack, and at point R located at $y=y_0$, midway between the stack and the resonator end (see Fig. 2). Point R is in the core of the resonator, far from the stack. For all values of the Mach number, it is observed (not shown) that velocity and temperature temporal variations remain sinusoidal at point R. Let us recall here that the standing wave in this computation is created by an incident wave that is reflected by the resonator end. The total time the wave spends in the resonator is less than one period and, hence, there is no sufficient time for the incoming wave to be deformed through nonlinear propagation. It is thus not surprising that the standing wave at point R is sinusoidal, even at high Mach number. This would probably not be the case for a complete (and straight) resonator driven by a source, such as a moving piston. But as was pointed out in the Introduction, the nonlinear behavior associated by the resonator is not of interest in the present work. At point M, the velocity is sinusoidal as well, but the temperature becomes inharmonic at high Mach numbers (this will be shown in a later figure), indicating a nonlinear behavior for the temperature. This behavior is responsible for a quasi saturation of the amplitude of the temperature oscillations at point M, which is shown in Fig. 8. This temperature saturation is the reason for the change of behavior of H_{xm} observed in Fig. 7: at low Mach number, both the velocity u' and the temperature T' vary with the Mach number M_a, so that the mean enthalpy flux H_{xm}, which is proportional to the product $u'T'$, varies as the square

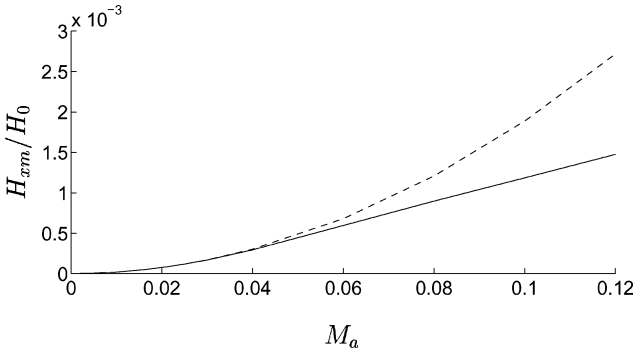

Fig. 7 Variation of the total enthalpy flux H_{xm} carried along an isothermal plate with the Mach number M_a: ——, calculated H_{xm} and – – –, M_a^2 fitting at low Mach numbers.

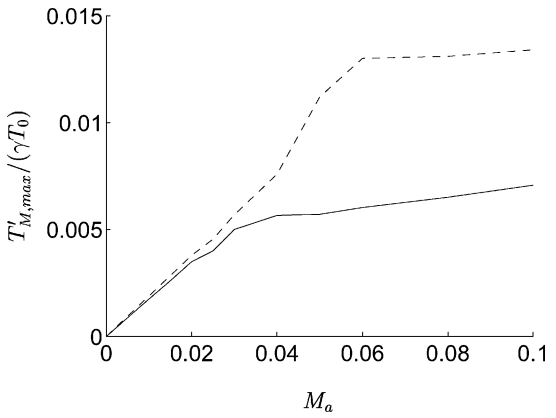

Fig. 8 Variation of the amplitude $T'_{M,\max}$ of temperature oscillation at point M with the Mach number M_a, for two plate lengths: ——, $L=\lambda/40$ and – – –, $L=2\lambda/40$.

of the Mach number, M_a^2. At high Mach numbers, the velocity u' varies with M_a, but the temperature T' saturates and remains nearly constant, so that the enthalpy flux H_{xm} varies with M_a. This nonlinear effect appears in the stack (point M) but not in the resonator (point R); thus, it is not due to a nonlinear propagation effect but to an interaction with the stack. In particular, and unfortunately, it is expected to occur even in inharmonic resonators,[22] which have a linear behavior. The nonlinear deformation and the saturation of temperature oscillations are affected by two parameters. First, at a fixed position of the plate (that is, a fixed value of kx_s), the Mach number at which the quasi saturation occurs depends on the plate length L. This is shown in Fig. 8 where the saturation occurs later for a plate with $L=2\lambda/40$ compared with the case of a plate with $L=\lambda/40$. For a very short plate, the saturation Mach number can be very low. Second, for a plate of fixed length, the position of the plate is another important parameter. The Mach number at which quasi saturation of temperature occurs decreases when the plate is moved toward the velocity antinode. This could be the reason for the observation made by Atchley et al.[7] that the temperature gradient generated in stack plates is better predicted by linear theory near the pressure antinode than near the velocity antinode.

The temperature oscillations near the edge of the plate were studied. The temporal variations of the temperature over two acoustic cycles are plotted for different values of the Mach number and for two different locations in the domain in Fig. 9, corresponding to point M, and in Fig. 10, corresponding to the the grid point located just above C. Constant values $\delta_\kappa/y_0=0.37$ and $kx_s=2.13$ are taken. For $M_a=0.005$, the temporal variations of the temperature at points C and M are sinusoidal. For $M_a=0.01$, the fluctuations at point M are still sinusoidal, whereas they have a U shape at point C. For larger Mach numbers, nonlinear deformation is observed at point M (this deformation leads to a saturation of the amplitude, as described in the preceding paragraph) and deformation at point C is

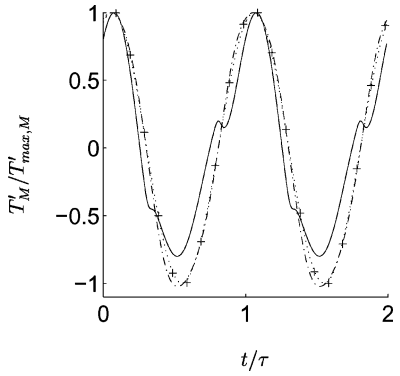

Fig. 9 Time variation of temperature at point M for different Mach numbers: +, $M_a = 0.005$; · · · ·, $M_a = 0.01$; - - - -, $M_a = 0.04$; and ——, $M_a = 0.08$.

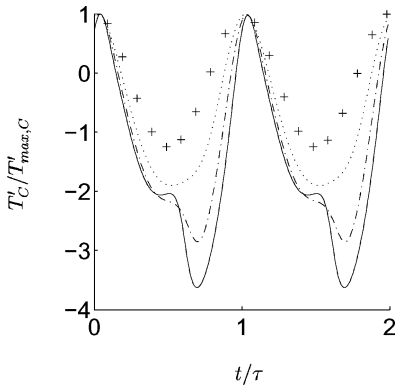

Fig. 10 Time variation of temperature at grid point located just above C (near the plate edge) for different Mach number: +, $M_a = 0.005$; · · · ·, $M_a = 0.01$; – – –, $M_a = 0.04$; and ——, $M_a = 0.08$.

much larger. Hence, the temperature oscillations at the edges of the plate are highly nonlinear. This tends to confirm that there is indeed temperature harmonic generation at the edges of the plate, which has been predicted analytically by Gusev et al.[23] and is due to the transition from an adiabatic behavior outside the plate to an isothermal behavior on the plate surface.

To conclude, the simulation of an isothermal plate has been performed. The isothermal model is a simplified one for a stack plate, but it may be useful as a benchmark problem. The model is much more realistic when a heat exchanger is involved. The model allowed some simple comparisons with other theoretical and numerical results while keeping the computation time reasonable. Some important nonlinear behaviors were observed. It is noteworthy that similar effects have also been observed[21] in the case of a more realistic nonisothermal model, which is presented in the next section. Hence, the isothermal model appears to be not too restrictive.

Results for a Nonisothermal Plate

In this section, the case of a nonisothermal plate with no heat exchangers is discussed. The temperature of the plate was calculated via Eq. (17) rather than prescribed. As previously mentioned, a nonisothermal plate simulation is costly because a temperature gradient develops in the plate, which requires some time. At least 300 acoustic cycles were necessary to reach a steady state compared to 50 acoustic cycles for an isothermal plate. To decrease the transient duration, one method is to use a small value of E in Eq. (17), but large enough so that the plate temperature does not oscillate during an acoustic cycle. (Using Swift's notation,[1] ϵ_s is kept small.) With E small, conduction of heat in the plate is small, which represents an ideal situation for practical devices. To simulate more realistic conditions, one possibility for increasing the heat conduction in the plate is to multiply K_s in Eq. (17) by a constant, α_s. In the following, $\alpha_s = 1$ unless specified otherwise, and $E/\delta_v = 0.05$.

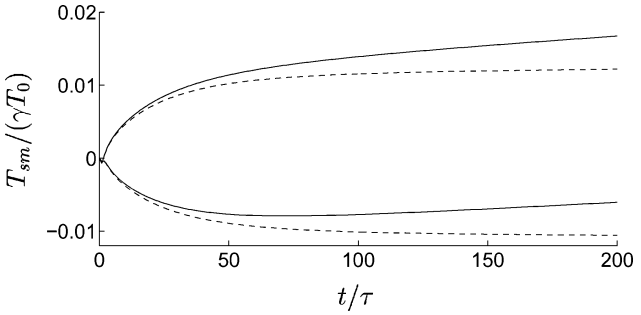

Fig. 11 Temperature of the plate as a function of time at point C (negative temperatures) and H (positive temperatures): ——, simulation including viscous dissipation and – – –, simulation without viscous dissipation.

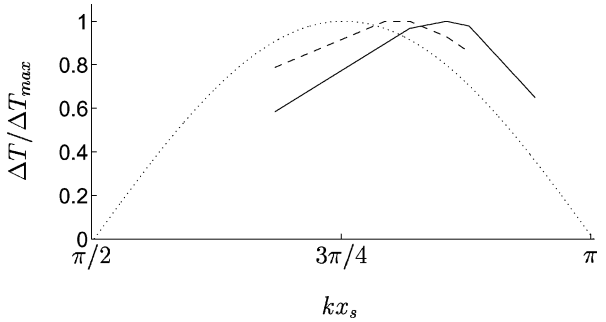

Fig. 12 Temperature difference between the extremities of the plate: – – –, $M_a = 0.02$; ——, $M_a = 0.04$; and · · · ·, prediction for very small M_a.

Using a low-heat-capacity plate allows the observation of the effects of viscous dissipation. These effects are usually relatively small, but in the absence of heat exchangers they lead to a uniform heating of the plate. This has been observed in experiments.[24,25] In these experiments, the temperature of the cold side of a plate immersed in a resonator was recorded. The temperature first decreased due to thermoacoustic heat pumping, and then increased due to the viscous heating. This increase was stronger when the plate was located near the velocity antinode. The hot side is heated by viscous dissipation at the same rate as the cold side. As a result, although the cold side temperature is increasing, the temperature difference between cold and hot sides of the plate is stationary. Two simulations were made for the same plate, with and without the viscous dissipation term Φ in Eq. (14). The following values were used: $\delta_\kappa/y_0 = 0.37$, $kx_s = 2.13$, and $M_a = 0.02$. The mean temperatures, $T_{\rm sm}(C)$ and $T_{\rm sm}(H)$, at the extremities C and H of the plate are plotted in Fig. 11 as a function of time for both simulations. Without viscous dissipation, the temperatures at points C and H both converge to a steady state. When viscous dissipation is included these temperatures drift. However, the temperature difference $\Delta T = T_{\rm sm}(H) - T_{\rm sm}(C)$ at the end of the calculation is the same for both simulations. Note that heating is observed after only 200 acoustic cycles because E is small.

The temperature difference $\Delta T = T_{\rm sm}(H) - T_{\rm sm}(C)$ was investigated as a function of the position of the plate for $\delta_\kappa/y_0 = 0.37$ and $\alpha_s = 20$. In Fig. 12, ΔT normalized by its maximum value $\Delta T_{\rm max}$ (when the position is varied) is plotted as a function of position represented by kx_s for different Mach numbers. ($kx_s = \pi$ at the end of the resonator.) The low-Mach-number prediction has a maximum for $kx_s = 3\pi/4 = 2.35$ that is between the pressure antinode and velocity antinode. The optimal position for the stack moves toward the resonator end as the Mach number increases, as expected from linear theory.[7]

Results with a Plate and Heat Exchangers

Two heat exchangers modeled by isothermal plates were added to the plate of the previous section. The temperatures of the hot and cold heat exchangers were prescribed as indicated in Eqs. (3)

and (4). The effect of these temperatures, as well as geometrical parameters, on the performance of the refrigerator were investigated. In the following, $T_h - T_0 = T_0 - T_c$, $G_h = G_c$, and $L_h = L_c$.

To measure the performance of the refrigerator, the cooling power, $Q_{c,m}$, is calculated by integrating h_{ym}^{cold} over the cold heat exchanger surface, where h_{ym}^{cold} is the value of h_{ym} given by Eq. (24) when the temperature gradient is calculated at the cold exchanger:

$$Q_{c,m} = \int_{S_c} h_{ym}^{\text{cold}}(x)\,\mathrm{d}x \tag{26}$$

Equivalent quantities, h_{ym}^{hot} and $Q_{h,m}$, can be defined at the hot heat exchanger. The mean acoustic power $W_m(x)$ at position x is obtained by integrating the average acoustic energy flux over the channel cross section:

$$W_m(x) = \int_{y=0}^{y=y_0} \langle p'(x, y)u'(x, y)\rangle_t\,\mathrm{d}y \tag{27}$$

The acoustic power absorbed by the refrigerator, $W_{m,0}$, is simply the value of W_m calculated over the surface S_{inout}; that is, $W_{m,0} = W_m(x_{\text{inout}})$. The total mean heat Q_m that is carried in the x direction is defined by

$$Q_m(x) = \int_{y=0}^{y=y_0} \rho_0 T_0 \langle u'(x, y)s'(x, y)\rangle_t\,\mathrm{d}y \tag{28}$$

where s is the entropy.

As an example, the axial variation of $H_{xm}(x)$, $W_m(x)$, and $Q_m(x)$ is shown in Figs. 13 and 14 for one typical calculation. Three regions may be distinguished on these figures.

First, in the region between the surface S_{inout} and the cold heat exchanger ($x/\delta_\nu < 0$), $W_m = W_{m,0}$ is constant. The heat flux Q_m is zero: no heat is carried outside the region of the plate/heat exchangers. The energy flux H_{xm} is simply equal to the work flux: $H_{xm} = W_m = W_{m,0}$. In this part of the resonator, a traveling wave is superimposed with the standing wave, such that the work $W_{m,0}$ provided to the plate by the wave is not zero. (In a pure standing wave there is no work flux.)

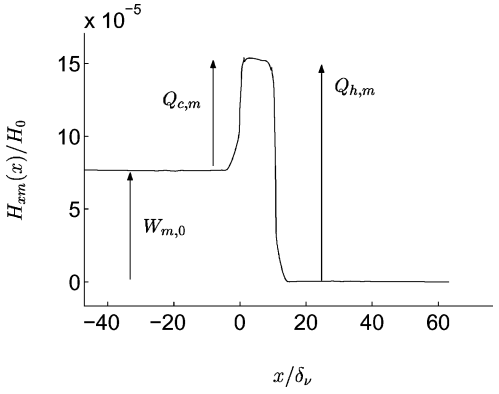

Fig. 13 Axial variation of total enthalpy flux: $x = 0$ is at the edge of the cold heat exchanger located toward S_{inout}.

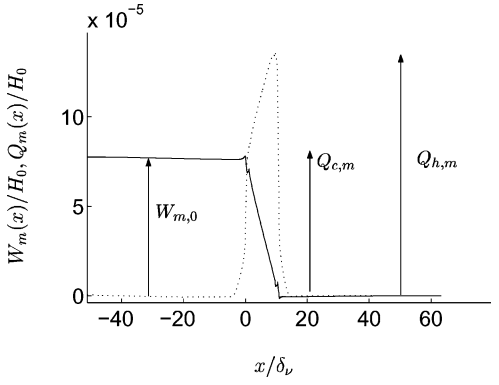

Fig. 14 Axial variation of total work flux and total heat flux: ——, $W_m(x)/H_0$; · · · ·, $Q_m(x)/H_0$; $x = 0$ is at the edge of the cold heat exchanger located toward S_{inout}.

Second, between the two heat exchangers ($0 < x/\delta_\nu < 12$), at the cold heat exchanger the value of Q_m increases suddenly by the amount $Q_{c,m}$ that is received from the exchanger. Past the cold heat exchanger, along the plate, W_m decreases linearly, whereas Q_m increases linearly, because work is transformed into heat by the plate. The enthalpy flux H_{xm}, which is equal to $Q_m + W_m$ (neglecting heat conduction), remains constant: $H_{xm} = W_{m,0} + Q_{c,m} = Q_{h,m}$. Just before the hot heat exchanger the value of Q_m reaches $Q_{h,m}$. At the hot heat exchanger $Q_{h,m}$ is transferred to the exchanger, and past this exchanger, $Q_m = 0$.

Finally, in the region between the hot heat exchanger and the end of the resonator ($x/\delta_\nu > 12$), $Q_m = 0$, there is no thermoacoustic effect outside the region of plate/heat exchangers, and $W_m = 0$, which means that a nearly perfect standing wave exists in this part of the resonator.

The coefficient of performance (COP) of the refrigerator is defined as

$$\text{COP} = Q_{c,m}/W_{m,0} \tag{29}$$

The maximum value of the COP that corresponds to an isentropic operation is given by the Carnot coefficient of performance (COPC), defined by

$$\text{COPC} = T_c/(T_h - T_c) \tag{30}$$

Finally the relative coefficient of performance (COPR) of the refrigerator is given by

$$\text{COPR} = \text{COP}/\text{COPC} \tag{31}$$

First the effect of temperatures T_c and T_h was studied. Constant values $M_a = 0.04$, $\delta_\kappa/y_0 = 0.37$, $k_x s = 2.13$, $L_c/L = 0.2$, and $G_c/L = 0.1$ were used. In Fig. 15 the cooling power is plotted as a function of T_c/T_h. The cooling power $Q_{c,m}$ is a linear function of T_c/T_h. For a value of T_c/T_h that is small, $Q_{c,m}$ is negative, which means that heat flows from the fluid to the heat exchanger because power is not sufficient to pump heat at a too-cold temperature T_c.

The COPR is plotted as a function of the temperature difference between the two heat exchangers in Fig. 16. The COPR has a maximum value. It was observed that this maximum occurs at a

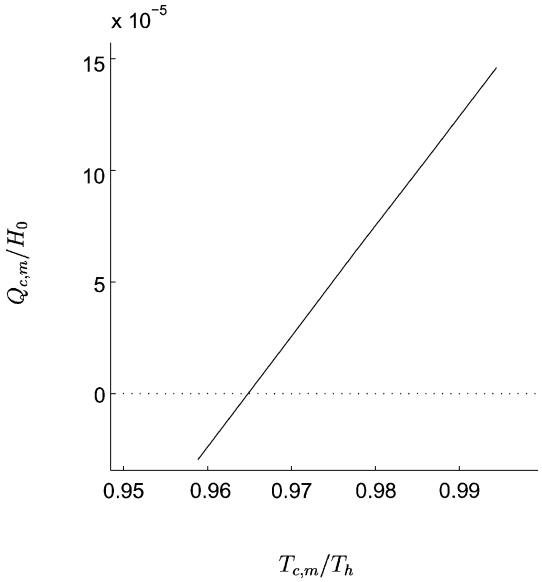

Fig. 15 Cooling power $Q_{c,m}$ as a function of the ratio of heat exchanger temperatures.

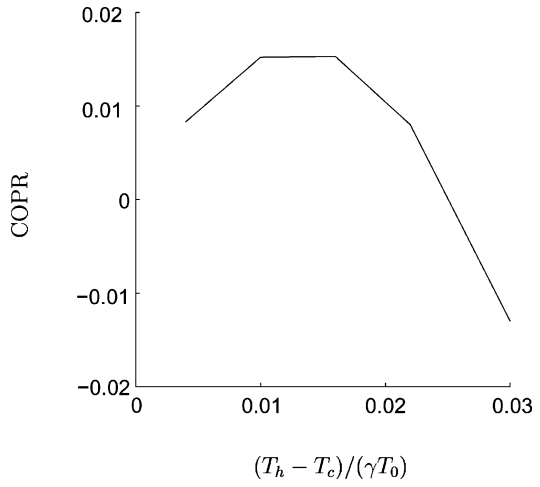

Fig. 16 COPR as a function of temperature difference between the two heat exchangers.

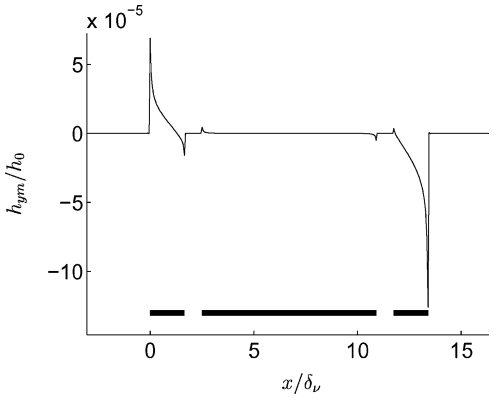

Fig. 17 Mean heat flux h_{ym} at $y = 0$ for $(T_h - T_c)/(\gamma T_0) = 0.016$. Origin $x = 0$ on the left edge of the cold heat exchanger. Thick lines at the bottom represent the plate and the heat exchangers.

temperature difference that is nearly the one that would exist between the two extremities of the plate if the heat exchangers were suppressed.

Up to here in this section only the global quantity of heat extracted from the cold heat exchanger was considered. It is interesting to look at the local mean heat flux. In Fig. 17, h_{ym} along the $y = 0$ boundary is plotted to capture the local mean heat flux at the two exchangers and at the plate.

First, note that h_{ym}^{plate} has very small absolute values compared with h_{ym}^{cold} and h_{ym}^{hot}. The plate induces a thermoacoustic heat transport in the x direction but there is little heat exchange between the fluid and the plate in the y direction. It can be seen that h_{ym}^{cold} has a nonuniform value over the cold heat exchanger surface and peaks at the edge away from the plate. Finally, h_{ym}^{cold} has a negative value at the edge of the cold heat exchanger facing the plate. This reverse heat flux at the cold exchanger reduces refrigerator performance. This was also observed in earlier studies of both thin exchangers[19] as well as thick exchangers.[12]

Another point of interest was the study of the effect of geometrical parameters: first, the gap between the plate and the cold heat exchanger, G_c, and the length of the cold heat exchanger, L_c, were varied. The position of the plate was kept constant at $kx_s = 2.13$. The following values were chosen: $(T_h - T_c)/(\gamma T_0) = 0.016$, $M_a = 0.04$, and $\delta_\kappa/y_0 = 0.37$. An important quantity is the particle displacement amplitude d_a, computed according to

$$d_a = u_M/2\pi f \tag{32}$$

where u_M is the amplitude of the velocity u at point M. It is well known that the heat exchanger length as well as the gap between the plate and the heat exchanger must have a length that is of the order of the particle displacement.[1] The aim was to study the evolution of cooling power and COPR as G_c and L_c vary around d_a.

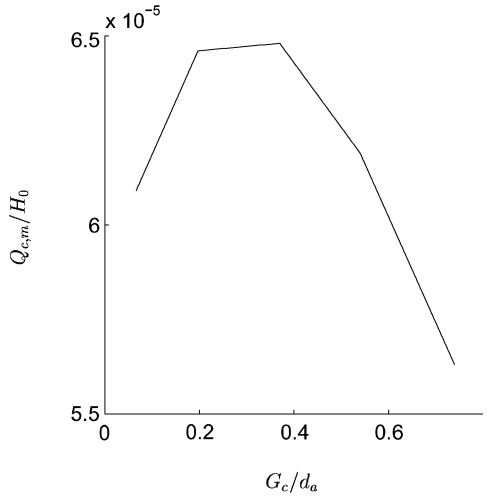

Fig. 18 Cooling power vs the gap $G_{c,m}$ between the plate and the cold heat exchanger; $L_c/d_a = 0.72$.

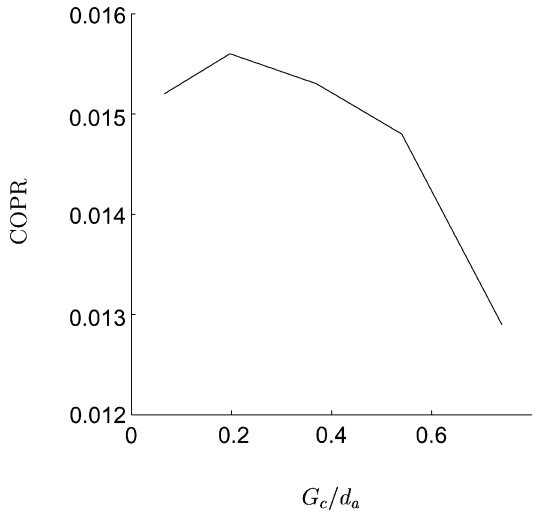

Fig. 19 COPR vs the gap G_c between the plate and the cold heat exchanger; $L_c/d_a = 0.72$.

In Figs. 18 and 19, the cooling power and the COPR are plotted as a function of the gap between the cold exchanger and the plate. The length of the cold heat exchanger is kept constant at $L_c/L = 0.2$, which corresponds to $L_c/d_a = 0.72$, and the gap G_c/L varies between 0.02 and 0.2. The cooling power reaches a maximum for $G_c/d_a \sim 0.4$. The COPR reaches a maximum for $G_c/d_a \sim 0.2$. The decrease of $Q_{c,m}$ and COPR at low values of G_c/d_a seems to be due to the reversed heat flux on the portion of the cold heat exchanger facing the stack. For the smallest value of G_c/d_a, the reverse heat flux at the cold heat exchanger is 17% that of the "nonreverse" heat flux. Hence, the maximum cooling power does not occur when there is no gap between the plate and the heat exchanger. This was predicted theoretically.[26] The dependencies of $Q_{c,m}$ and COPR on L_c/d_a are very similar. The cooling power is plotted in Fig. 20 as a function of L_c/d_a for a constant value $G_c/L = 0.1$, which corresponds to $G_c/d_a = 0.36$. The normalized heat exchanger length, L_c/L, varies between 0.05 and 0.6. For a too-small value of L_c/d_a, the exchanger surface is too small and the cooling power remains low, and so the efficiency is low. When L_c/d_a is large, once again, $Q_{c,m}$ (and hence the COPR) diminishes due to a reverse heat flux on the portion of the cold heat exchanger facing the stack.

Finally the effects of channel height y_0 were studied. Constant values $L_c/L = 0.2$ and $G_c/L = 0.1$ were imposed (corresponding

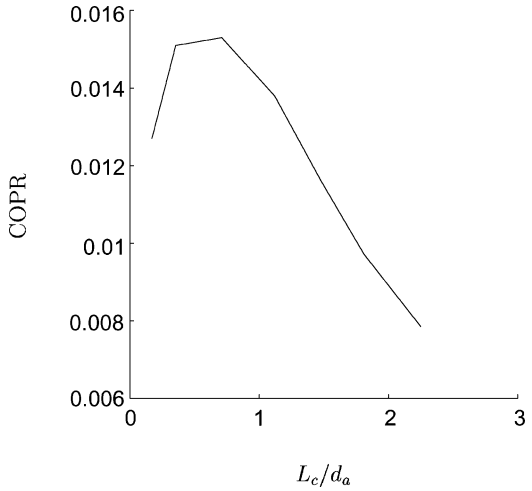

Fig. 20 COPR vs the length L_c of the cold heat exchanger; $G_c/d_a = 0.36$.

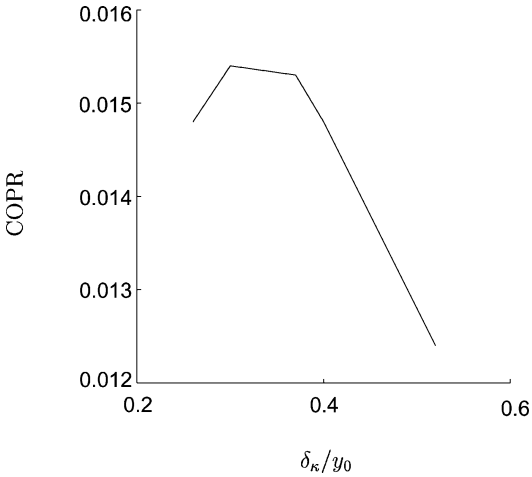

Fig. 21 COPR vs the height δ_κ/y_0 of the domain; $G_c/d_a = 0.36$ and $L_c/d_a = 0.72$.

to $L_c/d_a = 0.72$ and $G_c/d_a = 0.36$), and the parameter δ_κ/y_0 was varied. The same values as before were used for other parameters: $kx_s = 2.13$, $(T_h - T_c)/(\gamma T_0) = 0.016$, and $M_a = 0.04$. The COPR is plotted as a function of δ_κ/y_0 in Fig. 21. Again there is an optimal value for this parameter, which is $\delta_\kappa/y_0 \sim 0.3$. Moreover, the value for which the cooling power is the highest is $\delta_\kappa/y_0 = 0.37$ (not shown). This is less than the value of 0.75 that was found previously for the isothermal plate and for a lower Mach number (see Fig. 5).

Note that, in the preceding calculations, the relative efficiency is typically 1.5%, which is small. There are several reasons for this. First, the plate is located at $kx_s = 2.13$ although the optimal position for the same Mach number is about $kx_s = 2.7$. For a plate located at $kx_s = 2.4$, the highest relative efficiency was 6% (not shown). Second, as concluded from this study, each parameter (L_c, G_c, y_0) must be chosen carefully. And of course these parameters and some others (L_h, G_h, L, M_a, x_s) should be chosen simultaneously, which has not been done here. For example, the optimum value $G_c/d_a \sim 0.4$ is correct for $L_c/d_a = 0.72$ but could be different for another value of L_c/d_a. Hence, to get an optimal efficiency a parametric study has to be made by varying all the parameters simultaneously. The important conclusion here is that G_c or L_c must be close to d_a, but a bad choice around this value can severely decrease the efficiency of the refrigerator.

Conclusions

Numerical simulations of flow and heat transfer in the vicinity of a zero-thickness stack plate and heat exchangers within a high-amplitude acoustic standing wave were performed. Nonlinear effects could be observed in the simplest case of an isolated isothermal plate. They consist of nonsinusoidal temperature oscillations at the edges of the plate, for any Mach number, and of nonlinear distortion of the temperature oscillations above the plate at relatively high Mach numbers. This induces a saturation of the temperature amplitude. These effects, not taken into account by available linear theory, have important consequences on the performance of the device. In particular, at high Mach numbers, the total energy flux carried along the plate is proportional to the Mach number rather than to the square of the Mach number. This effect is stronger near the velocity antinode and for short plates. Interestingly, these nonlinear effects are not due to acoustic nonlinear propagation in the resonator and appear in the stack region only. Heat exchangers were included and the effect of operating and geometrical parameters on the refrigerator performance was studied. It was found that both the cold heat exchanger length and the gap between the cold heat exchanger and the plate must be close to the particle displacement amplitude, but a poor choice around this value can decrease refrigerator efficiency.

Acknowledgments

The authors acknowledge the French Ministry of Defense (Délégation Générale pour l'Armement) for its financial support. Calculations were partially performed using the Institut du Développement et des Ressources en Informatique Scientifique computing center. The authors also acknowledge Luc Mongeau for helpful discussions.

References

[1]Swift, G. W., "Thermoacoustic Engines," *Journal of the Acoustical Society of America*, Vol. 84, No. 4, 1988, pp. 1145–1180.

[2]Garrett, S. L., Adeff, J. A., and Hofler, T. J., "Thermoacoustic Refrigerator for Space Applications," *Journal of Thermophysics and Heat Transfer*, Vol. 7, No. 4, 1993, pp. 595–599.

[3]Backhaus, S., and Swift, G. W., "A Thermoacoustic-Stirling Engine: Detailed Study," *Journal of the Acoustical Society of America*, Vol. 107, No. 6, 2000, pp. 3148–3166.

[4]Poese, M. E., and Garrett, S. L., "Performance Measurements on a Thermoacoustic Refrigerator Driven at High Amplitudes," *Journal of the Acoustical Society of America*, Vol. 107, No. 5, 2000, pp. 2480–2486.

[5]Waxler, R., "Stationary Velocity and Pressure Gradients in a Thermoacoustic Stack," *Journal of the Acoustical Society of America*, Vol. 109, No. 6, 2001, pp. 2739–2750.

[6]Atchley, A. A., Bass, H. E., and Hofler, T. J., "Development of Nonlinear Waves in a Thermoacoustic Prime Mover," *Frontiers of Nonlinear Acoustics: 12th ISNA*, edited by M. F. Hamilton and D. T. Blackstock, Elsevier, New York, 1990, pp. 603–608.

[7]Atchley, A. A., Hofler, T. J., Muzerall, M. L., Kite, M. D., and Ao, C., "Acoustically Generated Temperature Gradients in Short Plates," *Journal of the Acoustical Society of America*, Vol. 88, No. 1, 1990, pp. 251–263.

[8]Worlikar, A. S., and Knio, O., "Numerical Simulation of a Thermoacoustic Refrigerator. Part 2: Stratified Flow Around the Stack," *Journal of Computational Physics*, Vol. 144, 1998, pp. 299–324.

[9]Cao, N., Olson, J. R., Swift, G. W., and Chen, S., "Energy Flux Density in a Thermoacoustic Couple," *Journal of the Acoustical Society of America*, Vol. 99, No. 6, 1996, pp. 3456–3464.

[10]Ishikawa, H., and Mee, D. J., "Numerical Investigations of Flow and Energy Fields near a Thermoacoustic Couple," *Journal of the Acoustical Society of America*, Vol. 111, No. 2, 2002, pp. 831–839.

[11]Worlikar, A. S., and Knio, O., "Numerical Simulation of a Thermoacoustic Refrigerator. Part 1: Unsteady Flow Around the Stack," *Journal of Computational Physics*, Vol. 127, 1998, pp. 424–451.

[12]Besnoin, E., "Numerical Study of Thermoacoustic Heat Exchangers," Ph.D. Dissertation, Dept. of Mechanical Engineering, Johns Hopkins Univ., Baltimore, MD, 2001.

[13]Blanc-Benon, Ph., Besnoin, E., and Knio, O., "Experimental and Computational Visualization of the Flow Field in a Thermoacoustic Stack," *Comptes Rendus Mecanique*, Vol. 331, No. 1, 2003, pp. 17–24.

[14]Karpov, S., and Prosperetti, A., "A Nonlinear Model of Thermoacoustics Devices," *Journal of the Acoustical Society of America*, Vol. 112, Vol. 4, 2002, pp. 1431–1444.

[15]Hamilton, M. F., Ilinskii, Y. A., and Zabolotskaya, E. A., "Nonlinear Two-Dimensional Model for Acoustic Engines," *Journal of the Acoustical Society of America*, Vol. 111, No. 5, 2002, pp. 2076–2086.

[16]Boluriaan, S., and Morris, P. J., "Numerical Prediction of Minor Losses in High Amplitude Acoustic Resonators," AIAA Paper 2002-2594, June 2002.

[17]Schneider, T., Botta, N., Geratz, K. J., and Klein, R., "Extension of Finite Volume Compressible Flow Solvers to Multi-Dimensional, Variable Density Zero Mach Number Flows," *Journal of Computational Physics*, Vol. 155, 1999, pp. 248–286.

[18]Chen, R., Chen, Y., Chen, C. T., and DeNatale, J., "Development of Miniature Thermoacoustic Refrigerators," AIAA Paper 2002-0206, Jan. 2002.

[19]Besnoin, E., and Knio, O., "Numerical Study of Thermoacoustic Heat Exchangers in the Thin Plate Limit," *Numerical Heat Transfer Part A—Applications*, Vol. 40, No. 5, 2001, pp. 445–471.

[20]Bogey, C., and Bailly, C., "A Family of Low Dispersive and Low Dissipative Explicit Schemes for Flow and Noise Computations," *Journal of Computational Physics*, Vol. 194, 2004, pp. 194–214.

[21]Marx, D., "Simulation Numérique d'un Réfrigérateur Thermoacoustique," Ph.D. Dissertation, Laboratoire de Mecanique des Fluides et d'Acoustique, No. 2003-34, Ecole Centrale de Lyon, Lyon, France, 2003.

[22]Lawrenson, C. C., Lipkens, B., Lucas, T. S., Perkins, D. K., and Van Doren, T. W., "Measurements of Macrosonic Standing Waves in Oscillating Closed Cavities," *Journal of the Acoustical Society of America*, Vol. 104, No. 2, 1998, pp. 623–636.

[23]Gusev, V., Lotton, P., Bailliet, H., Job, S., and Bruneau, M., "Thermal Wave Harmonics Generation in the Hydrodynamical Heat Transport in Thermoacoustics," *Journal of the Acoustical Society of America*, Vol. 109, No. 1, 2001, pp. 84–90.

[24]Duffourd, S., "Réfrigérateur Thermoacoustique: Études Analytiques et Expérimentales en Vue d'une Miniaturisation," Ph.D. Dissertation, Laboratoire de Mecanique des Fluides et d'Acoustique, No. 2001-06, Ecole Centrale de Lyon, Lyon, France, 2000.

[25]Blanc-Benon, Ph., "High Amplitude Effects in Thermoacoustic Refrigerators," *Nonlinear Acoustics at the Beginning of the 21st Century*, edited by O. V. Rudenko and O. A. Sapozhnikov, Vol. 1, 16th International Symposium on Nonlinear Acoustics, Moscow, 2002, pp. 171–178.

[26]Gusev, V., Lotton, P., Bailliet, H., Job, S., and Bruneau, M., "Relaxation-Time Approximation for Analytical Evaluation of Temperature Field in Thermoacoustic Stack," *Journal of Sound and Vibration*, Vol. 235, No. 5, 2000, pp. 711–726.

A. Karagozian
Associate Editor